OPTICAL ARRAY ASPECTS OF COMPUTED SPECTROSCOPY™

Ralph T. Hoctor[a], Frederick W. Wheeler[a] and Eamon B. Barrett[b]

[a] GE Global Research, Niskayuna NY, USA 12309
E-mail: {hoctor, wheeler}@research.ge.com

[b] Lockheed Martin Space Systems, ATC, Sunnyvale, CA, USA 94089
E-mail: eamon.barrett@lmco.com

ABSTRACT

Computed Spectroscopy™ (CS) is a new approach to hyperspectral imaging recently introduced by the authors [1]*. The CS technique uses an adjustable optical array, which can be considered to be a form of delay-and-sum passive beamformer. Adopting this point of view, such an array can be analyzed using the (difference) coarray [2], and a previous publication by the present authors [1] features a brief coarray-based analysis. In the present paper we review the Computed Spectroscopy method, give a coarray-based analysis of the approach, show how numerical problems arise in the reconstruction of wavenumber spectra at low spatial frequencies and give a method for addressing these problems in the computation. Additionally, we discuss an improved approach to discretization of the image formation model.

1. INTRODUCTION

Computed Spectroscopy™ (CS) [1] is a new approach to hyperspectral imaging for satellite remote sensing that makes use of an array of optical subapertures, each of which can be finely adjusted to vary the distance between the subaperture and the image formation plane. Such sparse optical arrays have long been considered for satellite imaging [3, chapter 36] and were recently used as the basis of a Fourier transform spectroscopy (FTS) approach to division-of-wavefront imaging spectroscopy [4,5] by splitting the aperture into two parts. The split aperture technique was experimentally verified in [6]. Unlike the FTS approach of [4], Computed Spectroscopy is intrinsically an imaging method; FTS is the point-by-point application of a well-known method for scalar spectroscopy. Additionally, and unlike FTS, CS allows independent use of the subapertures, which in turn allows computation of wavenumber spectra at higher special frequencies than the approach given in [4]. (The high frequency content of the CS hyperspectral image is the same as that obtained by division-of-amplitude FTS.)

Briefly, the CS™ method makes use of the fact that an optical array with adjustable subaperture optical path lengths can synthesize image point spread functions (PSF's) that vary with wavenumber. This means that regions of the image with different reflectance spectra will have different PSF's, and an ensemble of panchromatic images, each with its own setting of the subapertures, can be used to reconstruct the wavenumber content of a scene by inverting a standard image formation model in the spatial frequency domain [1]. FTS, either division-of-wavefront or division-of-amplitude, also performs computations on an ensemble of panchromatic images, but the rationale for forming the images is different from that of CS. Because of the dependence on a spatially varying PSF, low spatial frequency regions of the scene, where the effects of differing PSF's cannot be distinguished, are not well estimated. This is also the case with division-of-wavefront FTS [5]. On the other hand, the division-of-wavefront approachs (including CS) have an SNR advantage over the use of a Michelson or other division-of-amplitude interferometer.

Computed Spectroscopy™ structures hyperspectral image formation as an image reconstruction (inverse) problem. In Section 2 of this paper we review CS and give a coarray analysis of the dimension of the system to be inverted in the reconstruction. This analysis points out a computational problem for low spatial frequencies, which is the result of bias in the induced weights. In Section 3 we give two numerical procedures for the estimation of the wavenumber spectra in the presence of low-pass bias, based on two different discretizations of the model, and in Section 4 we summarize the results.

2. COMPUTED SPECTROSCOPY USING OPTICAL ARRAYS

The CS method is based on the following model for the formation of a panchromatic image. The intensity image due to a monochromatic wavefield with wavenumber k is given by the convolution of the PSF at wavenumber k with the intensity source distribution, $S(\mathbf{x},k)$, which is the hyperspectral data to be imaged. The panchromatic

* Lockheed Martin patent pending.

image is a superposition of narrowband images over the wavenumber passband, K:

$$I(\mathbf{x}) = \int_K I(\mathbf{x};k)\, dk = \int_K [P(\mathbf{x};k) * S(\mathbf{x},k)]dk \qquad (1)$$

(See the appendix of the recent paper by Thurman and Fienup [5].)

The narrowband PSF at k, P(**x**;k), can be written as the Fourier transform of the autocorrelation of the aperture apodization function, C(**w**;k), which is an unnormalized version of the optical transfer function (OTF):

$$P(\mathbf{x};k) = \int_{CA} C(\mathbf{w};k)\, e^{\frac{-jk}{z}\mathbf{w}^T\mathbf{x}}\, d\mathbf{w} \qquad (2)$$

where the integration region, denoted by CA, is defined to be the (difference) coarray of the aperture [2]. Expressing the convolution in (1) as a product in the spatial Fourier transform domain gives

$$I(\mathbf{x}) = \int_K \int_{CA_{\lambda z}} C(\lambda z\mathbf{v};k)\, \tilde{S}(\mathbf{v},k)\, e^{-j2\pi\,\mathbf{v}^T\mathbf{x}}\, d\mathbf{v}\, dk \qquad (3)$$

where $\tilde{S}(\mathbf{v};k)$ is the inverse spatial Fourier transform of $S(\mathbf{x},k)$ and the limit of integration $CA_{\lambda z}$ represents integration over the image of the coarray in the spatial frequency domain under the mapping $\mathbf{v} = \mathbf{w}/\lambda z$. In the spatial frequency domain $CA_{\lambda z}$ is the support of the inverse spatial transform of the narrowband PSF at wavelength λ. Taking the spatial Fourier transform (FT) of both sides of (3) gives the spatial FT of the panchromatic image as

$$\tilde{I}(\mathbf{v}) = \int_K C(\lambda z\mathbf{v};k)\, \tilde{S}(\mathbf{v},k)\, dk \qquad (4)$$

This expression gives the 2-D Fourier transform of a panchromatic image at a fixed spatial frequency as an inner product, in the wavenumber domain, between the spatial FT of the source and a weight function imposed by adjustment of the subaperture optical path length parameters. Because both functions are complex, (4) is actually the inner product of $\tilde{S}(\mathbf{v},k)$ and $C^*(\lambda z\mathbf{v};k)$.

If we take L panchromatic images using an N-subaperture optical array, the weight function in (4) for the q^{th} image can be expressed as [1]

$$C_q(\lambda z\,\mathbf{v};k) = \sum_{n=1}^{N}\sum_{m=1}^{N} e^{jk(D_n^{(q)} - D_m^{(q)})}\; X\left(\frac{2\pi z\,\mathbf{v}}{k} - (\mathbf{u}_n - \mathbf{u}_m)\right) \qquad (5)$$

for q=1,…,L and where X(.) is the spatial autocorrelation of the subaperture transmittance functions (assumed identical for all) which is located at a lag equal to the difference of the correlated subaperture centers, given by $\mathbf{u}_n$. The quantities $D_n^{(q)}$ in (5) are the adjustable distances from the n^{th} subaperture to the image formation plane for the q^{th} image and correspond to the delay in the delay-and-sum beamformer interpretation. Note that each term of the weight function sum is composed of an amplitude weight modulated by a segment of a complex exponential with frequency $(D_n^{(q)} - D_m^{(q)})$.

Using (5) in (4), we have L observed images, and the equations

$$\tilde{I}_q(\mathbf{v}) = \int_K C_q(\lambda z\,\mathbf{v};k)\, \tilde{S}(\mathbf{v},k)\, dk \qquad (6)$$

for q=1,…,L, can be solved for $\tilde{S}(\mathbf{v},k)$, which solution we denote by $\hat{\tilde{S}}(\mathbf{v},k)$. This is true even if $\{C_q^*\}$ is not a basis, in which case this set of equations can be solved in the least squares sense for the projection of $\tilde{S}(\mathbf{v},k)$ onto the space spanned by $\{C_q^*\}$. (As a practical matter, we need span only a finite dimensional subspace, since we will sample the wavenumber spectrum.) This is the approach taken in Computed Spectroscopy™, and the dimension of this space is of importance to the performance of the method.

Dimension of the Induced Basis.

From the point of view of array signal processing, the most salient feature of optical arrays is that the array elements are large. In our application, each array element is a telescope.

Figure 1 depicts a sample optical array and its coarray [2]. The array elements are annuli because of a mirror that partially blocks each element's aperture. Each of the circles away from the origin in the plot of Figure 1b is the support of the cross-correlation of two of the subapertures. The circle at the origin is the support of the autocorrelations of the subapertures. We call the circles coarray segments, and each one corresponds to one or more of the X(.) in (5). Each segment has its own modulating term, which can be controlled by the adjustable aperture.

The coarray plot shows that there is a great deal of redundancy for this configuration, especially near the origin. Redundancy means that the same point of the coarray plane is covered by multiple coarray segments.

For every bounded region in Figure 1b, there is a subset of the terms of the sum of (5) that contribute weight vectors to the spatial frequencies in that region. (Each bounded region has constant redundancy.) Note that the amplitude portion of each term of the sum of (5) is the same for every component image, and only the frequency terms can be changed by subaperture adjustment.

It is remarkable how much more complicated the coarray analysis is when the elements are large. Even though there are 37 distinct coarray segments in Fig 1b, there are literally hundreds of distinct regions with different redundancies and different induced weights. This makes the design problem for the $\{C_q\}$ difficult. For this reason we generate random sets of aperture

displacements and compare them for the dimension of the induced weights. We do this only on the grid of DFT coefficients (see Section 3), which limits the number of points at which a high-dimensional basis must be induced. Still, the bases are typically over-determined, with a number of weight vectors that is greater than the dimension.

The discussion suggests that the use of minimum or reduced redundancy arrays might simplify the specification of the weight vectors. This idea has not been investigated.

Bias at Low Spatial Frequencies.

Equation (4) for the induced weight vectors can be partitioned into two sums as in (7) to demonstrate the reconstruction degeneracy for low spatial frequencies.

$$C_q(\lambda z\,\mathbf{v};k)=\sum_{n=1}^{N} X\left(\frac{2\pi z\,\mathbf{v}}{k}\right) + \sum_{n=1}^{N}\sum_{\substack{m=1\\ m\neq n}}^{N} e^{jk\,(D_n^{(q)}-D_m^{(q)})}\; X\left(\frac{2\pi z\,\mathbf{v}}{k}-(\mathbf{u}_n-\mathbf{u}_m)\right) \tag{7}$$

The coarray segments at lag zero are all part of the first sum in (7); note that these are the same for all panchromatic images, no matter how the aperture is adjusted. The segments in the second sum overlap those in the first sum due to the redundancy depicted in Figure 1. To the extent that the subaperture edges are separated from each other, there is a small region around the origin that is not redundant. Only the mean value of the wavenumber spectrum can be reconstructed in this region; the same is true for the FTS approach of [4].

This inability to modulate the zero-lag segments results in the addition of the weight function given by the first term in (7) to every induced weight function given by the second sum of (7) for every spatial frequency in the zero-lag segment. The dimension of the induced basis is not affected by this, but the system can never be orthogonal under these circumstances and its inversion can be a poorly conditioned operation for the lowest spatial frequencies. Spatial frequencies outside the zero-lag segment are not affected.

In the next section we will give numerical procedures for the inversion of the system of (6) for all spatial frequencies, including those with bias terms.

3. Discretization and Numerical Procedure for the Zero-lag Segment

In order to solve the inverse problem numerically based on the forward system in (6), the inner products must be discretized in both spatial frequency and wavenumber. In spatial frequency, we do this by computing the DFT of each of the sampled component images. This takes the place of the spatial Fourier transform that produced (4), and results in an edge effect that has to be suppressed in the computed hyperspectral images [1].

For wavenumber discretization, we use the moment discretization of Nashed [7], which is different from the approach given in [1]. The new approach rests on the observation that the computed estimate of $\tilde{S}(\mathbf{v},k)$ will always be a linear combination of the $\{C_q\}$:

$$\hat{\tilde{S}}(\mathbf{v},k)=\sum_{q=1}^{L} b_q(\mathbf{v})\,C_q(\lambda z\mathbf{v};k) \tag{8}$$

and the estimation problem is equivalent to finding the $\{b_q\}$. The set of equations of (6) can be written in the form of a vector equality for the $\mathbf{n}^{th}$ DFT coefficient

$$\mathbf{\Phi_n}=\begin{bmatrix}\tilde{I}_1(\mathbf{n})\\ \vdots\\ \tilde{I}_L(\mathbf{n})\end{bmatrix}=\begin{bmatrix}\int_K C_1(\lambda z\mathbf{v}(\mathbf{n});k)\,\tilde{S}(\mathbf{v}(\mathbf{n}),k)\,dk\\ \vdots\\ \int_K C_L(\lambda z\mathbf{v}(\mathbf{n});k)\,\tilde{S}(\mathbf{v}(\mathbf{n}),k)\,dk\end{bmatrix} \tag{9}$$

where $\mathbf{v}(\mathbf{n})$ is the analog spatial frequency associated with the $\mathbf{n}^{th}$ DFT coefficient. This can be written as a matrix equation by substitution of the estimate in the form of (8) for the quantity $\tilde{S}(\mathbf{v}(\mathbf{n}),k)$ in (9):

$$\mathbf{\Phi_n}=\begin{bmatrix}\sum_{q=1}^{L} b_q\,c_{1,q}\\ \vdots\\ \sum_{q=1}^{L} b_q\,c_{L,q}\end{bmatrix}=\begin{bmatrix}c_{1,1} & \cdots & c_{1,L}\\ \vdots & \ddots & \vdots\\ c_{L,1} & \cdots & c_{L,L}\end{bmatrix}\begin{bmatrix}b_1\\ \vdots\\ b_L\end{bmatrix} \tag{10}$$

where we have suppressed the dependence of all the various terms on the righthand side in (10) on spatial frequency and have defined the inner products of the weight vectors as

$$c_{n,m}=\int_K C_n(\lambda z\,\mathbf{v}(\mathbf{n});k)\,C_m(\lambda z\,\mathbf{v}(\mathbf{n});k)\,dk \tag{11}$$

Using the obvious notation for (10), we have

$$\mathbf{\Phi_n}=\mathbf{C}\,\mathbf{b} \tag{12}$$

The matrix $\mathbf{C}$ need not be of full rank. In general, if the $\{C_q\}$ span a space of dimension X, then $\mathbf{C}$ will have rank X. In this case a pseudoinverse can be computed from the SVD that will allow us to express the least-squares solution to (9) in the form of (8).

The main advantage of moment discretization is that it requires no assumptions about the weight functions, as the approach of [1] did. As long as the numerical integration used to compute the integrals of (11) is accurate, no assumptions are required.

A discrete wavenumber spectrum estimate in the form of integrals over a partition of the wavenumber domain

$$\hat{\tilde{S}}_p=\int_{K_p}\tilde{S}(\mathbf{v}(\mathbf{n}),k)\,dk \tag{13}$$

can be computed from (8) by numerical integration over the set of bands $\{K_1,\ldots,K_p\}$ forming the partition.

Reconstruction with Bias Compensation.
In view of (7), within the zero-lag coarray segment equation (6) can be rewritten as

$$\tilde{I}_q(\mathbf{v}) = \int_K \left(C_q(\lambda z\mathbf{v};k) + B(\lambda z\mathbf{v};k)\right)\tilde{S}(\mathbf{v},k)\,dk \qquad (14)$$

where we have used the $\{C_q\}$ notation for the controllable part of the weight and added a second term to represent the bias. This holds everywhere on the coarray plane with the understanding that the bias is zero outside the zero-lag coarray segment. If substitute this equation into (9) and use the result to re-write (10), we get

$$\mathbf{\Phi_n} = \mathbf{C}\,\mathbf{b} + \left(\begin{bmatrix} c_{B,1} & \cdots & c_{B,L} \end{bmatrix} \begin{bmatrix} b_1 \\ \vdots \\ b_L \end{bmatrix} \right) \begin{bmatrix} 1 \\ \vdots \\ 1 \end{bmatrix} \qquad (15)$$

where we have defined

$$c_{B,q} = \int_K B(\lambda z\mathbf{v};k)\,C_q(\lambda z\mathbf{v};k)\,dk \qquad (16)$$

Denoting the row vector in (15) by $\mathbf{c}_B^T$ we have

$$\mathbf{\Phi_n} = \mathbf{C}\,\mathbf{b} + \left(\mathbf{c}_B^T\,\mathbf{b}\right)\mathbf{1}$$

If we multiply both sides by the pseudoinverse of $\mathbf{C}$ and recognize that the inner product is a scalar, we obtain

$$\mathbf{C}^+\,\mathbf{\Phi_n} = \mathbf{b} + \mathbf{C}^+\,\mathbf{1}\,\mathbf{c}_B^T\,\mathbf{b} = \left(\mathbf{I} + \mathbf{C}^+\,\mathbf{1}\,\mathbf{c}_B^T\right)\mathbf{b} \qquad (17)$$

where we note that the term in parenthesis is a rank-one update to the identity matrix. If we apply the partitioned matrix inversion lemma, we get:

$$\mathbf{b} = \left(I - \frac{\mathbf{C}^+\,\mathbf{1}\,\mathbf{c}_B^T}{1 + \mathbf{c}_B^T\,\mathbf{C}^+\,\mathbf{1}} \right) \mathbf{C}^+\,\mathbf{\Phi_n} \qquad (18)$$

assuming that $\mathbf{c}_B^T\,\mathbf{C}^+\,\mathbf{1} \neq -1$, which could be part of the design criteria for the $\{C_q\}$. This computation applies for all DFT frequencies, with the understanding that $\mathbf{c}_B = \mathbf{0}$ outside the zero-lag coarray segment.

4. DISCUSSION

In this paper we have reviewed the Computed Spectroscopy™ method presented in [1], and showed how bias arises in the computation of wavenumber spectra at low spatial frequencies. This analysis was framed in terms of the (difference) coarray, which is segmented into overlapping pieces, each with its own induced weights. The bias must be dealt with in the computation in order for acceptable results to be obtained, and a simple approach to this computation was given.

The same effect for low spatial frequencies occurs when the Fourier transform spectroscopy approach is applied to an optical array in split aperture mode [4,5,6]. In this scheme, every panchromatic component image represents a specific path length difference between the two parts of the aperture. According to (7), every such image has a low spatial resolution component corresponding to the zero-lag coarray segment. Thus, at a given image pixel, the ensemble of images represents the Fourier transform of the wavenumber power spectrum, plus a constant term. When the Fourier transform is performed, this constant part is mapped to the zeroth DFT coefficient. This component can be ignored, and so eliminated, provided that there is no leakage of the bias energy into other DFT bins. This is a well-known problem in classical spectrum estimation and is generally addressed through the use of a lag window [8]. The use of a lag window to lower the sidelobes of the analysis bin filters reduces the spectral resolution.

Thus, in order to prevent leakage while retaining resolution, the lag domain (that is, the set of path length differences) must be sampled over a larger range. However, in a hyperspectral imaging system, the range of the lag domain sampled is usually already limited by SNR. This is always a problem with hyperspectral imaging using FTS, but the presence of the unknown bias term adds an additional complication.

Note that is not advantageous to perform this bias removal operation prior to the FT since the bias comes from the image source and must be estimated. Recall that the zeroth DFT coefficient is equal to the sample mean, so that mean subtraction removes energy residing in the sidelobes of the zeroth DFT filter, producing an effect similar to leakage.

In general, Computed Spectroscopy™ has an advantage over FTS in that none of the component images are necessarily of low SNR, as are the high-lag images required for high-resolution image domain FTS. This is because of the difference in the fundamental method of representing or encoding the wavenumber spectral information in the panchromatic images. In CS™ this encoding is done through a variation of high-sidelobe image PSF, while in FTS, it is a per-pixel amplitude variation which tends towards zero at large lags.

The moment discretization approach of Section 3 is well-matched with CS in that the representation of the estimated spectra given in (8) retains the continuous nature of the induced weight functions. This is a primary point of contrast between CS and FTS. FTS starts with a sampled observation of the temporal autocorrelation for each pixel, and computes an estimated wavenumber spectrum by a DFT, while CS computes a projection onto a set of continuous basis functions and discretization of the spectral estimate follows.

Finally, we must emphasize that in any region near the origin of the coarray plane that is covered only by the zero-lag segment, only the mean value of the wavenumber spectrum can be computed. The computation of Section 3 applies only in regions that are redundantly covered by higher-lag coarray segments.

For many types of adjustable aperture, the optical array elements cannot be made to abut, and such a region will necessarily result.

ACKNOWLEDGEMENT

This report was prepared by GE GRC as an account of work sponsored by Lockheed Martin Corporation. Information contained in this report constitutes technical information which is the property of Lockheed Martin Corporation. Neither GE nor Lockheed Martin Corporation, nor any person acting on behalf of either; a. Makes any warranty or representation, expressed or implied, with respect to the use of any information contained in this report, or that the use of any information, apparatus, method, or process disclosed in this report may not infringe privately owned rights; or b. Assume any liabilities with respect to the use of, or for damages resulting from the use of, any information, apparatus, method or process disclosed in this report.

5. REFERENCES

[1] R.T. Hoctor, F.W. Wheeler and E.B. Barrett, "Computed Spectroscopy using segmented apertures," *Proc. 2006 SPIE Computational Imaging IV (SPIE vol. 6065),* C.A, Bouman, E.L. Miller, I. Pollak (Eds.), pp. 60650H:1-12 Jan. 2006.

[2] R.T. Hoctor and S.A. Kassam, "The unifying role of the coarray in aperture synthesis for coherent and incoherent imaging," *Proceedings of the IEEE*, vol. 78, pp. 735-752, April, 1990.

[3] G.O. Reynolds, J.B. DeVelis, G.B. Parrent, and B.J. Thompson, *The New Physical Optics Notebook: Tutorials in Fourier Optics*, SPIE Optical Engineering Press, 1989.

[4] R.L. Kendrick, E.H. Smith and A.L. Duncan, "Imaging Fourier transform spectrometry with a Fizeau interferometer," *Proc. SPIE Interferometry in Space Conference (4852)*, pp. 657-662, August, 2002.

[5] S.T. Thurman and J.R. Fienup, "Multi-aperture Fourier transform imaging spectroscopy: theory and imaging properties," *Optics Express*, vol. 13, pp. 2160-2175, March 2005.

[6] R.L. Kendrick, E.H. Smith, D.N. Christie, D.A. Bennett, D. Theil and E.B. Barrett, "Multiple-aperture imaging spectrometer: computer simulation and experimental validation," *Proc. 33d IEEE Applied Imagery Pattern Recognition Workshop*, pp. 3-9, Oct. 2004.

[7] C.K. Rushforth, "Signal restoration, functional analysis and Fredholm integral equations of the first kind," in *Image Recovery: Theory and Application*, H. Stark (Ed.), Academic Press, 1987.

[8] G.M. Jenkins and D.G. Watts, *Spectral Analysis and its Applications*, Holden-Day, 1968.

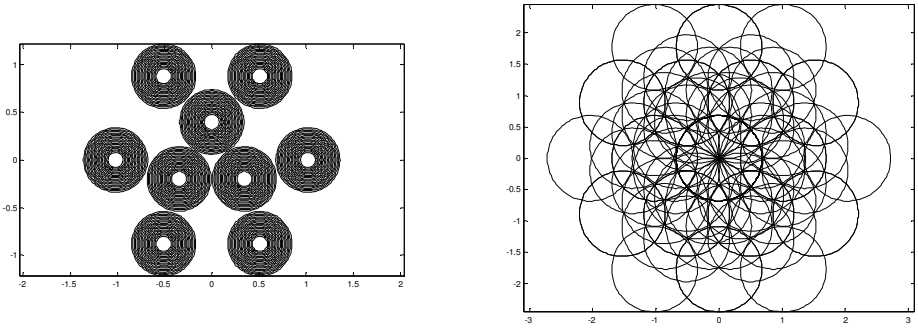

a. b.

Figure 1: a) array geometry, b) locations of coarray segments.